ISSN 2449-8955 European Journal of Biological Research *Research Article*

DOI: http://dx.doi.org/10.5281/zenodo.7041808

In silico exploration of *Lycoris* alkaloids as potential inhibitors of SARS-CoV-2 main protease (Mpro)

Fredrick M. Musila [1,*], Grace W. Gitau [1], Magrate M. Kaigongi [2], Dickson B. Kinyanyi [1], Jeremiah M. Mulu [3], Joseph M. Nguta [4]

[1] School of Biological and Life Sciences, Technical University of Kenya, PO Box 52428-00200, Nairobi, Kenya

[2] Kenya Forestry Research Institute, PO Box 20412-00200, Nairobi, Kenya

[3] Department of Chemistry, College of Biological and Physical Sciences, University of Nairobi, PO Box 30197-00100, Nairobi, Kenya

[4] Department of Public Health, Pharmacology and Toxicology, Faculty of Veterinary Medicine, University of Nairobi, PO Box 29053-00625, Nairobi, Kenya

* Corresponding author e-mail: musila@tukenya.ac.ke

Received: 03 April 2022; **Revised submission:** 12 August 2022; **Accepted:** 31 August 2022

https://jbrodka.com/index.php/ejbr

ABSTRACT: Coronavirus disease 2019 (COVID-19) is a pandemic whose adverse effects have been felt all over the world. As of August 2022, reports indicated that over 500 million people in the world had been infected and the number of rising deaths from the disease were slightly above 6.4 million. New variants of the causative agent, SARS-CoV-2 are emanating now and then and some are more efficacious and harder to manage. SARS-CoV-2 main protease (Mpro) has essential functions in viral gene expression and replication through proteolytic cleavage of polyproteins. Search for SARS-CoV-2 Mpro inhibitors is a vital step in the treatment and management of COVID-19. In this study, we investigated whether alkaloids with antiviral and myriad other bioactivities from the genus *Lycoris* can act as SARS-CoV-2 Mpro inhibitors. We conducted a computer-aided drug design study through screening optimal ligands for SARS-CoV-2 Mpro from a list of over 150 *Lycoris* alkaloids created from online databases such as ChEMBL, PubChem, ChemSpider, and published journal papers. The *In silico* study involved molecular docking of *Lycoris* alkaloids to SARS-CoV-2 Mpro active site, absorption, distribution, metabolism, elimination and toxicity (ADMET) screening and finally molecular dynamic (MD) simulations of the most promising ligand-SARS-CoV-2 Mpro complexes. The study identified 3,11-dimethoxy-lycoramine, narwedine, O-demethyllycoramine and epilycoramine as drug-like and lead-like *Lycoris* alkaloids with favorable ADMET properties and are very likely to have an inhibition activity on SARS-CoV-2 Mpro and may become potential drug candidates.

Keywords: *Lycoris* alkaloids; SARS-CoV-2 Mpro; Molecular docking; ADMET screening; Molecular dynamic simulations; Ligand-receptor interactions.

1. INTRODUCTION

COVID-19 is caused by severe acute respiratory syndrome coronavirus 2 (SARS-CoV-2) which is a positive-sense, single-stranded RNA virus that belongs to the family *Coronaviridiae* [1]. According to World Health Organization reports, COVID-19 was declared a global pandemic after spreading to different regions

around the world. Its current subsequent global spread has been associated with over 400 million confirmed infections and over 5 million deaths [2]. The phylogenetic relationship of full-length SARS-CoV-2 and bat coronavirus RaTG13 suggests bats as probable reservoir hosts [3], however, the disease has now progressed to be transmitted primarily by human-to-human contact with respiratory secretions, such as droplets[4]. The high infection rates and deaths caused by COVID -19 have impeded the economic growth of various countries. Furthermore, some countries have experienced a burden on their healthcare system due to an abrupt increase in the number of patients who need to be hospitalized [5].

Although substantial effort has been made towards identifying antivirals for SARS-CoV-2, the current vaccines have been met with imminent challenges such as low production capacity that does not meet the worldwide demand and lack of affordability by low and middle-income countries [6]. Moreover, the development of an effective vaccine is at an unprecedented fast pace and the use of new technologies adopted has raised a lot of safety issues worldwide. Therefore, the current vaccines have been deployed with various unresolved concerns that only the course of time will shed light on the perception of the vaccine in terms of safety and acceptance. Furthermore, it remains to be elucidated whether the current vaccines have high efficacy against the viral variants that have emerged [7]. It is for these reasons that it is still of great importance to develop safe, effective, affordable and readily available antiviral vaccines or drugs that can be used to prevent the high mortality caused by SARS-CoV-2.

Coronavirus main protease (Mpro) and papain-like protease (PLpro) have essential functions in viral gene expression and replication through proteolytic cleavage of polyproteins [8]. SARS-CoV-2 Mpro also termed 3-chymotrypsin-like protease (3CLpro) has recently received a lot of attention from researchers as a potential drug target for the development of effective antiviral therapies for the treatment of COVID-19 infection [9, 10]. SARS-CoV-2 open reading frame 1 (ORF 1a) and ORF1ab which are located at the 5' terminus of the genome encodes polyproteins pp1a and pp1ab respectively. The pp1a contains 10 nonstructural proteins (nps) whereas pp1ab contains 15 nps which perform important functions on the survival of the virus [11]. SARS-CoV-2 Mpro specifically cleaves these two large overlapping polyproteins pp1a and pp1ab to functional proteins and this auto-processing step is crucial during the SARS-CoV-2 replication cycle [10,12]. From this perspective, the proteolytic activity positions Mpro as a key enzyme in virus replication and its inhibition would block SARS-CoV-2 replication [10]. Accordingly, viral-encoded proteases have previously emerged as successful antiviral drug targets against chronic infections caused by viruses such as the human immunodeficiency virus or hepatitis C virus [13].

Unlike PLpro, the Mpro proteolytic activity is exclusively located on polypeptide sequence after amino acid glutamine and this positions Mpro as an ideal potential drug target because there are no reported human cell proteases with a similar cleavage specificity [10,14]. Moreover, inhibition of proteolytic activity of Mpro has been suggested to be unlikely toxic due to its substrate specificity property [14]. Several compounds such as α-ketoamide, velpatasvir and antineoplastic drug carmofur have recently been reported to inhibit SARS-CoV-2 replication through their SARS-CoV-2 Mpro inhibitory roles [9,15,16]. However, the toxicity and antiviral molecular inhibitory mechanisms of these compounds and drugs remain questionable.

Lycoris Herbert, is a genus in the family Amaryllidaceae comprising of about 20 species that are native to the warm temperate areas of eastern Asia such as China, Taiwan, Japan and Korea [17]. *Lycoris* species have been widely used in traditional medicine to treat various diseases such as sore throats, cancer, purulent wounds, blisters, mastitis, tympanitis, ulcers, poliomyelitis and neurodegenerative diseases [18,19]. Consequently, *Lycoris* species have been subjected to extensive phytochemical and pharmacological investigations, resulting

in the isolation or identification of a rich source alkaloids belonging to different structural types [17]. *Lycoris* alkaloids have been reported to have promising and interesting bioactivities such as antiproliferative [18], anti-inflammatory and antimalarial activities [20,22], neuroprotective activity [23,24], antitrypanosomal activity [22], acetylcholinesterase-inhibiting activity [24], antibacterial, antitumor, antifungal, analgesic, cytotoxic, cholinesterase inhibition activities [17], and antiviral activity against several viruses such as poliomyelitis virus, herpes simplex virus (type I), dengue virus, SARS-CoV as well as SARS-CoV-2 in *in vitro* studies [16]. Alkaloids of different structural types such as lycorine-type, homolycorine-type, haemanthamine type, narsiclasine-type, tazzetine-type, montenine-type and galanthamine-type alkaloids have been identified in *Lycoris* species[19,25,26]. Notable species in the genus whose alkaloids have been identified and investigated for various bioactivities include: *Lycoris radiata* [27], *L. aurea, L. straminea, L. sprengeri*, *L. longituba* [28], *L. caldwelli* [29], *L. guangxiensis* [26], *L. traubii* [22], *L. albiflora*, *L. chinensis*, *L. haywardii*, *L. incarnata* and *L. squamigera* [25].

Over 150 alkaloids have been isolated from *Lycoris* genus and a majority of their identities have been verified and are available in various chemical databases such as PubChem, ChemSpider and ChEMBL. Currently, there are no studies that have reported *in silico* or *in vivo* anti-SARS-CoV-2 properties of these promising *Lycoris* alkaloids through their inhibitory role by interaction with SARS-CoV-2 Mpro. Therefore, the current study sought to use an *in silico* approach to investigate whether the reported alkaloids from *Lycoris* species are potential inhibitors of the novel SARS-CoV-2 coronavirus through interaction with SARS-CoV-2 Mpro. Molecular docking, ADMET-related *in-silico* models and molecular dynamic simulations were utilized for screening of the potential anti-SARS-CoV-2 *Lycoris* alkaloids through interaction with SARS-CoV-2 Mpro. Overall, the outcome of this study lays a foundation for the search for anti-SARS- CoV-2 remedies from the most promising alkaloids in the genus *Lycoris*.

2. MATERIALS AND METHODS

2.1. Ligand database creation

Alkaloids reported from various *Lycoris* species were obtained majorly from PubChem and ChEMBL databases [30,31] between April and May 2021. For those alkaloids not found in any of the chemical databases but only found in various literature materials, their structures were illustrated in ChemDraw Ultra 8 [32] and all file conversions were done in Biovia Discovery Studio [33] eventually leading to the creation of a database of 186 *Lycoris* alkaloids. Medicinal chemistry was the main criteria used in the selection of compounds through screening for lead-likeness and subjecting *Lycoris* alkaloids to PAINS and Brenk checks. PAINS identifies compounds that are likely to interfere in screening technologies in a number of ways particularly through protein reactivity. Such compounds may be suggestive of a selective and optimizable hit but they represent poor choices for drug development [34]. PAINS online remover [35] was used to screen for such pan assay interference compounds from the database of *Lycoris* alkaloids used in this study. Brenk screening involves checking whether compounds consist of or can form any of 105 structural fragments described by Brenk et al. [36] believed to be putatively toxic, chemically reactive, metabolically unstable, or bear properties responsible for poor pharmacokinetics. SwissADME returned Brenk warnings if such moieties were found in the *Lycoris* alkaloids under evaluation [37].

2.2. Ligands/receptor preparation and molecular docking

Lycoris alkaloids that passed the PAINS and Brenk screening were selected for molecular docking. Selected alkaloids (ligands) together with the SARS-CoV-2 Mpro 3D structure obtained from Protein Data Bank, PDB ID: 6XBG were prepared in UCSF Chimera [38]. Ligands were added hydrogens and charges while SARS-CoV-2 MPro was prepared by removal of water and the co-crystalized ligand UAW246 and other heteroatoms. Identification of the active sites of SAR-CoV-2 Mpro was done in BIOVIA Discovery Visualizer. Molecular docking was done using AutoDock Vina in PyRx [39] by superposing prepared ligands on the active site of the SARS-CoV-2 Mpro receptor within the AutoDock Vina search space, the number of independent docking runs were set at 9 for each complex. The co-crystalized ligand UAW246 was also included in the docking studies as the positive control. The resulting complexes were visualized in Biovia Discovery Visualizer to identify various binding energies of the various poses and the best docking pose from each complex with favorable interactions.

2.3. ADMET screening

The created database was then subjected to ADMET screening using SwissADME [37] and ADMETSAR [40] programs. Each compound was screened for lipophilicity, water-solubility, oral drug absorption, pharmacokinetics such as gastrointestinal (GI) absorption, Blood Brain Barrier (BBB) permeation, skin permeability and cytochrome P450 enzymes inhibition, drug-likeness and physicochemical parameters such as the number of rotatable bonds, fraction of carbons in the sp3 hybridization. Number of hydrogen bond acceptors, number of hydrogen bond donor, molar refractivity and topological polar surface area of each alkaloid was also investigated.

2.4. Molecular dynamic simulations

Molecular dynamic (MD) simulations were done using the GROMACS simulation package in WebGro, which is a fully automated online tool for performing molecular dynamic simulations of macromolecules alone or in complex with ligands (https://simlab.uams.edu/index.php). Mpro is functionally dimeric enzyme consisting of Chain A and Chain B [41]. Only chain A of the Mpro dimer was employed for MD simulations because the targeted active site was on Chain A. It has been proposed that there is an asymmetry in SARS-CoV-2 Mpro functioning and only one binding site is active at a time and ligand binding at one cavity induces conformational changes on the ligand-free pocket that renders it inactive. Hence, it is advisable to remove any other chain and remain with only the chain of interest during molecular docking and MD simulations [9]. Selected complexes that had favorable binding scores and interactions were converted into PDB format and ligand topology files generated using the PRODRG server [42]. Ligand topology files were uploaded alongside their corresponding complexes in Webgro MD simulation tool. GROMOS96 43a1 was selected as force field type, flexible simple point-charge water model was used, box type was triclinic and 0.15M NaCl was added. Under energy minimization, steepest descent was selected at 5000 steps while under equilibration and MD simulation run parameters; pressure of 1 bar, NVT/NPT pressure equilibration type and temperature of 300K, leapfrog MD integrator were selected. The number of frames per simulation was set at 1000 and MD simulation was set to run for 100 nanoseconds (ns) in WebGro to determine the root mean square deviation (RMSD) of the given structure, root mean square fluctuation (RMSF), the radius of gyration, or structural compactness (Rg), Solvent accessible surface area (SASA) and number of H-bonds in each frame over time.

3. RESULTS AND DISCUSSION

3.1. Molecular docking

Lycorine is one of the widely studied *Lycoris* alkaloids and has been reported to have myriad bioactivities including antiviral activities especially the fact that it has been argued to have anti-SARS-CoV-2 activity [43], however, it didn't pass the PAINS and Brenk checks because it can form potentially toxic alkene moieties. Toxic interactions of lycorine with host ribosomes in the management of SARS-CoV-2 have indeed been reported by Ren [43], and hence it was not selected for molecular docking. Out of 186 *Lycoris* alkaloids investigated in the current study, only 17 were selected for molecular docking and ADMET screening after PAINS and Brenk checks. Molecular docking results which include binding energies of the various complexes, amino acids showing hydrogen bonds, hydrophobic bonds and other interactions are shown in Table 1. The more negative the binding energy is, the better the docking score/binding score.

Compounds that had high number of hydrogen bond interactions with SARS-CoV-2 Mpro included 7-oxodihydrolycorine, lycoricidine and 7-deoxynarciclasine with 6 hydrogen bonds, lycoramine, dihydrolycorine, and cherylline with 5 hydrogen bonds while epilycoramine and narciclasine interacted with SARS-CoV-2 Mpro through 7 hydrogen bonds. Co-crystallized ligand UAW246 which was used as the positive control interacted with Mpro through 4 hydrogens bonds. A higher number of hydrogen bonds in the protein-ligand complex is favorable and enhance ligand-receptor interactions leading to high binding score or lower binding energy [53]. Besides, all the compounds interacted with the receptor through various hydrophobic and other interactions which also contributed to the overall binding score of each ligand-Mpro complex. The highest docking score of- 7.9 kcal mol^{-1} was observed in UAW246-Mpro complex, followed by second highest docking score of - 7.7 kcal mol^{-1} in 7-oxodihydrolycorine-Mpro complex while the lowest docking score of -6.0 $kcalmol^{-1}$ was observed in assoanine-Mpro complex. The complex or the pose with the best binding score may not always be selected for further exploration because the best binding score is not a reliable criterion for the selection of the best solution in common docking applications as argued by Ramírez and Caballero [54]. It is strongly recommended to choose the best docking solution for further studies such as MD simulations based on the interactions involved and additional structural criteria described for the ligand under investigation [54]. The most common amino acids which formed hydrogen bonding with *Lycoris* alkaloids were GLU166, CYS145, SER144, GLN189 and GLY143. These are conserved residues in the active site of SARS-CoV-2 Mpro as reported by Yoshino et al. [55] hence any ligand interacting with these residues has the potential of inhibiting SARS-CoV-2 Mpro.

3.2. ADMET properties of Lycoris alkaloids

Selected *Lycoris* alkaloids were drug-like and fulfilled Lipinski (Pfizer) filter, the pioneer rule-of-five [56], Ghose (Amgen) [57], Veber (GSK) [58], Egan (Pharmacia) [59] and Muegge (Bayer) [60] filters for prospective oral drugs. The above five filters have varying cut-offs for lipophilicity, molecular size, polarity, saturation and number of rotatable bonds for potential drugs. The topological polar surface area of selected *Lycoris* alkaloids ranged from between 20 and 130 $Å^2$, their molar refractivity ranged from 40 to 130 m^3mol^{-1} and the fraction of carbons in the sp3 hybridization was not less than 0.25. They were all soluble in water (log S was not higher than 6) and were lead-like compounds whose molecular weight ranged from 250 to 350 daltons. ADMET predicted profiles of the seventeen selected *Lycoris* alkaloids are displayed in Tables 2, 3 and 4.

Table 1. Binding energies and ligand-receptor interactions.

***Lycoris* alkaloid**	**Source**	**Alkaloid-Mpro Complex Binding energy [ΔG bind(kcalmol^{-1})]**	**Amino acids that interact with compounds through hydrogen bonds**	**Amino acids that make hydrophobic and other Interactions (van der Waals, pi-sigma bonds, alkyl, pi-alkyl, Pi-Anion, Pi-Pi T-shaped, Pi-Sigma)**
O-demethyllycoramine	[44]	-7.2	SER144, HIS 163, GLU166, GLN189	PHE140, CYS145, HIS164, MET165, HIS41, ASN142, LEU141
7-oxodihydrolycorine	[19]	-7.7	GLN189, ASN142, GLY143, YS145, SER144, LEU141	MET49, THR25, HIS163, MET165, GLU166
7-deoxynarciclasine	[45]	-7.2	MET165, CYS145, HIS163(2), SER144, PHE140	HIS172, LEU141, GLU166, ASN142,
5,6-dihydro-5-methyl-2-hydroxyphenanthridine	[20]	-6.7	GLU166, SER144, LEU141, THR190	GLN189, GLU166, ASN142, CYS145, HIS163, HIS164, MET165
3,11-dimethoxy-lycoramine	[26]	-7.1	GLU166(2), PHE140, CYS145	HIS41, GLN189, ASP187, HIS164, MET165, HIS172, HIS163, LEU141, SER144, ASN142, GLY143
(2R)-2-methoxy-1,2,3,4-tetrahydro [1,3] dioxolo[4,5-j] phenanthridine	[46]	-6.7	CYS145, HIS164, ASN142, THR190	MET165, ARG189, GLN189, LEU141, PHE140, GLU166, HIS163
Zephyranthine	[47]	-7.1	GLU166, LEU141, CYS145	GLN189, MET165, ARG188, ASP187, HIS164, HIS41, CYS145, HIS163, SER144, PHE140, GLY143, ASN142
Lycoramine	[48]	-6.6	GLU166(2), PHE140, CYS145, HIS164	MET145, HIS172, SER144, LEU141, HIS163, GLY143, ASN142, GLN189, HIS41, ASP187, ARG188
Lycoricidine	[49]	-7.0	THR190(2), ARG188, GLU166, CYS145, LEU141	PRO168, ALA191, GLN192, GLN189, MET165, HIS164, CYS145, GLY143, ASN142, SER144
Perlolyrine	[24]	-7.2	GLU166(2), PHE140, HIS164	PRO168, MET165, CYS145, ASN142, SER144, HIS163, HIS172, LEU141, HIS41, GLN189, THR190, ALA191
Dihydrolycorine	[27]	-7.2	GLU166(2), HIS164, CYS145, LEU141	ASN142, PHE140, SER144, GLY143, HIS163, ASP187, HIS41, ARG188, GLN189, MET165
Anhydrolycorine	[25]	-6.9	CYS145	TYR54, ARG188, ASP187, GLN189, MET165, HIS164, GLU166, LEU141, ASN142, GLY143, CYS145, HIS41, MET49
Assoanine	[25]	-6.0	GLY143, THR26	ASN142, THR25, LEU27, HIS41, CYS145, MET49, HIS164, MET165, GLN189, GLU166
Cherylline	[25]	-6.7	GLU166, ASN142, GLY143, SER144, PHE140	PRO168, LEU167, HIS172, HIS163, LEU141, GLN189
Epilycoramine	[50]	-6.9	GLU166, ASN142, HIS163, SER144, HIS164, GLN189(2)	PHE140, LEU141, HIS41, MET165, CYS145
Narciclasine	[51]	-7.6	GLU166, CYS145, HIS163(2), SER144, ASN142, GLN189	THR190, MET165, HIS164, CYS145, PHE140, LEU141
Narwedine	[52]	-6.7	GLU166	MET165, HIS164, GLN189, HIS41, CYS145, MET49, ASN142, LEU141, HIS163, SER144, HIS172, PHE140
UAW246	Co-crystallized with PDB ID:6XBG	-7.9	HIS41, SER144, HIS163, PHE140	HIS164, MET165, GLN189, THR190, ALA191, PRO168, THR26, THR25, CYS145, LEU27, GLY143, ASN142, GLU166, LEU141, HIS172

3.2.1. Predicted absorption and distribution

Under absorption, all selected compounds except narciclasine had high GI absorption, negative log Kp (cm/s) values implying low skin permeability and all were soluble with their log S ranging from -4 to -2 [37] (Table 2). Predicted absorption across the intestinal epithelium showed that all ligands had CaCo2 permeability except 7-oxodihydrolycorine, 7-deoxynarciclasine, lycoricidine, perlolyrine and narciclasine. The plasma protein binding (PPB) ranged from the lowest value of 41.3% in O-demethyllycoramine to the highest value of 96.9% in 5,6-dihydro-5-methyl-2-hydroxyphenanthridine. On the other hand, the distribution of selected compounds indicated that they could all pass through the BBB except 7-oxodihydrolycorine, 7-deoxynarciclasine, zephyranthine, lycoricidine, dihydrolycorine, narciclasine. Although very small molecules may just pass through the BBB, this uncontrolled passage into the brain may not be desirable and strategies are being developed for controlled passage as well as targeted drug delivery to the brain [61].

All selected alkaloids can act as P-glycoprotein (P-gp) substrates except 7-deoxynarciclasine, lycoricidine and narciclasine (Table 2). P-gp is involved in the transport of different classes of drugs such as antineoplastic drugs which include docetaxel, etoposide, vincristine sulphate and calcium channel blockers like amlodipine, cyclosporin, digoxin and erythromycin [62]. Drugs that induce P-gp such as rifampicin, can reduce the bioavailability of some other drugs in the body while P-gp inhibitors may increase the bioavailability of P-gp susceptible drugs. It has also been reported that many drugs transported by P-gp can also be metabolized by cytochrome P4503A4 [63]. P-gp is important in the efflux of drugs through biological membranes, for instance from the gastrointestinal wall to the lumen or from the brain. Indeed, one major role of P-gp is the protection of the central nervous system from xenobiotics [64].

3.2.2. Cytochrome P450 inhibition

Cytochrome P450 (CYP) isoenzymes play a key role in drug elimination through metabolic biotransformation [65]. CYP enzymes and P-gp can process small molecules synergistically to improve the protection of tissues [66]. The five major CYP isoforms which are substrates for about 90% of all therapeutic molecules include: CYP1A2, CYP2C19, CYP2C9, CYP2D6, CYP3A4 as reported by Daina et al. [37]. Inhibition to any of the major cytochrome P450 isoenzymes results in pharmacokinetics-related drug-drug interactions which can lead to toxicity or other undesirable adverse effects due to lower clearance and accumulation of the drug [67]. Some compounds may inhibit all or specific CYP isoenzymes and it is important to predict the degree with which the potential drug molecule will inhibit the CYP isoenzymes by determining the isoenzymes likely to be affected [68]. Preferable drugs are those that are P-gp substrates that don't inhibit the majority of CYP isoenzymes notably CYP3A4 and CYP2D6 which are the most significant in drug elimination [69]. Most of the compounds under study inhibited specific CYP isoenzymes. From the prediction studies, 7-oxodihydrolycorine, 7-deoxynarciclasine, lycoricidine, epilycoramine, narciclasine and narwedine did not inhibit any of the CYP isoenzymes while cherylline, dihydrolycorine, lycoramine, zephyranthine, 3,11-dimethoxy-lycoramine and O-demethyllycoramine inhibited only CYP2D6 (Table 3).

3.2.3. Pharmacokinetic inhibitors and medicinal chemistry

All the selected compounds were not multidrug and toxin extrusion 1 (MATE1) inhibitors, they also did not inhibit OATP2B1 but inhibited both OATP1B1 and OATP1B3 organic anion uptake transporters (Table 3). MATE1 is highly expressed in the kidney, adrenal gland, liver, skeletal muscle and several other tissues.

Table 2. Predicted drug-likeness, absorption and distribution of *Lycoris* alkaloids.

			Drug-likeness			Absorption			Distribution		
Name	**Formula**	**MW**	**Consensus Log P/ Lipophilicity**	**Lipinski suitability**	**GI absorption**	**Skin permeability/ log Kp (cm/s)**	**Solubility/ Log S**	**Caco2 permeability**	**Plasma Protein B**	**BBB permeant**	**P-gp substrate**
O-demethyllycoramine	C16H21NO3	275.15	1.77	Yes	High	-6.82	Soluble	+	0.413	Yes	Yes
7-oxodihydrolycorine	C16H17NO6	319.31	-0.01	Yes	High	-8.75	Soluble	-	0.814	No	Yes
7-deoxynarciclasine	C14H13NO6	291.26	-0.42	Yes	High	-9.04	Soluble	-	0.814	No	No
5,6-dihydro-5-methyl-2-hydroxyphenanthridine	C15H13NO3	255.27	2.35	Yes	High	-5.94	Soluble	+	0.969	Yes	Yes
3,11-dimethoxy-lycoramine	C17H23NO3	289.37	2.07	Yes	High	-6.67	Soluble	+	0.654	Yes	Yes
(2R)-2-methoxy-1,2,3,4-tetrahydro[1,3]dioxolo[4,5-j]phenanthridine	C15H15NO3	257.28	2.51	Yes	High	-6.08	Soluble	+	0.835	Yes	Yes
Zephyranthine	C16H20NO4	290.33	1.05	Yes	High	-7.54	Soluble	+	0.77	No	Yes
Lycoramine	C17H23NO3	289.37	2.09	Yes	High	-6.67	Soluble	+	0.654	Yes	Yes
Lycoricidine	C14H13NO6	291.26	-0.42	Yes	High	-9.04	Soluble	-	0.725	No	No
Perlolyrine	C16H12N2O2	264.28	2.55	Yes	High	-6.33	Soluble	-	0.78	Yes	Yes
Dihydrolycorine	C16H19NO4	289.33	1.09	Yes	High	-7.53	Soluble	+	0.77	No	Yes
Anhydrolycorine	C16H13NO2	251.28	2.89	Yes	High	-5.64	Soluble	+	1.124	Yes	Yes
Assoanine	C17H17NO2	267.32	3.01	Yes	High	-5.64	Soluble	+	0.855	Yes	Yes
Cherylline	C17H19NO3	285.34	2.34	Yes	High	-6.26	Soluble	+	0.657	Yes	Yes
Epilycoramine	C17H23NO3	289.37	2.09	Yes	High	-6.67	Soluble	+	0.654	Yes	Yes
Narciclasine	C14H13NO7	307.26	-0.61	Yes	Low	-9	Soluble	-	0.828	No	No
Narwedine	C17H19NO3	285.34	2.01	Yes	High	-6.8	Soluble	+	0.49	Yes	Yes

It has been reported that MATE1 could play a role in the renal tubular secretion of cationic drugs in humans. MATE1 also acts as an efflux transporter of cellular substrates in other tissues [70]. Hence MATE1 is suitable for the distribution of drugs in tissues. In the kidney, MATE1 mediates the efflux of drugs from epithelial cells into urine [71]. On the other hand, OATP1B1 and OATP1B3 anion uptake transporters are exclusively expressed on the sinusoidal side of hepatocytes [72]. OATP1B1, OATP2B2 and OATP1B3 enhance metabolism through intestinal and hepatic uptake of a diverse array of xenobiotics from blood. In vitro and in vivo studies have shown that some drugs inhibit these transporters and cause clinically relevant drug-drug interactions [73,74]. As a large number of therapeutic reagents are substrates or inhibitors of OATP1B1 and OATP1B3, we should be aware of the extent of drug-dependent interactions caused by the inhibition of these transporters [74]. Since the severity of drug-dependent interactions may be minor or major, the FDA and EMA recommend in vitro testing of OATP1B1 and OATP1B3 interactions for drug candidates that are eliminated in part via the liver or are co-administered with substrates for these pharmacokinetic transporters [75].

Human organic cationic transporters (OCT1 and OCT2) are polyspecific transporters of small and hydrophilic organic cations, including toxic substances, endogenous compounds and clinically used drugs [76]. Among the OCT family, OCT1 is expressed mainly in the basolateral membrane of hepatocytes [77]. In the kidney, OCT2 is expressed on the basolateral membrane of the proximal tubule epithelium and is involved in the uptake of many cations and xenobiotics from the bloodstream into renal epithelial cells [78]. Selected alkaloids did not inhibit human organic cationic transporters (OCT1 and OCT2) except 5,6-dihydro-5-methyl-2-hydroxyphenanthridine, (2R)-2-methoxy-1,2,3,4-tetrahydro[1,3]dioxolo[4,5-j] phenanthridine, anhydrolycorine, assoanine and cheryline which inhibited OCT1. Assoanine is the only alkaloid which inhibited OCT2 (Table 3).

3.2.4. Predicted toxicity

Predicted Ames mutagenesis was negative for all compounds except 7-deoxynarciclasine, (2R)-2-methoxy-1,2,3,4-tetrahydro [1,3] dioxolo [4,5-j] phenanthridine, lycoricidine and perlolyrine where the test was positive (Table 4). AMES is a short-term bacterial reverse mutation assay and it is used to detect chemicals that can cause DNA damage leading to mutations [79]. For oral toxicity, all compounds fell under class III and only assoanine was placed under class II. Class III includes substances with chemical structures that permit a strong initial presumption of safety or may even suggest significant toxicity or have reactive functional groups. Class II includes substances that are less harmless than class I substances but do not contain structural features suggestive of toxicity like those substances in class III [80,81]. No eye irritation and corrosion were reported in all the compounds. Seven *Lycoris* alkaloids were predicted to be hepatotoxic, unlike the ten compounds which were predicted not to be hepatotoxic (Table 4).

Human Ether-à-go-go-Related Gene (hERG) is a gene that codes for a protein known as $K_v11.1$; the alpha subunit of a potassium ion channel [82]. This gene is important for cardiac repolarization and dysfunction. The hERG causes long QT syndrome and sudden death making its inhibition an important anti-target that must be avoided during drug design and drug development [83]. In the current study, most of the compounds did not inhibit the hERG gene except (2R)-2-methoxy-1,2,3,4-tetrahydro [1,3] dioxolo [4,5-j] phenanthridine, assoanine and cherylline (Table 4) hence further explorations of the three compounds should be avoided. A micronucleus test is used in toxicological screening for potential genotoxic compounds [84].

Table 3. Predicted metabolism and medicinal chemistry of *Lycoris* alkaloids.

	Metabolism											Medicinal chemistry			
	Cytochrome P450 inhibition					pharmacokinetics transporters inhibition									
Name	**CYP 1A2**	**CYP 2C19**	**CY P2C9**	**CYP 2D6**	**CYP 3A4**	**MATE 1**	**OATP 1B1**	**OATP 1B3**	**OATP 2B1**	**OCT1**	**OCT2**	**PAINS alerts**	**Brenk alerts**	**Lead-likeness**	**Synthetic availability**
O-demethyllycoramine	No	No	No	Yes	No	-	+	+	-	-	-	0	0	Yes	4.24
7-oxodihydrolycorine	No	No	No	No	No	-	+	+	-	-	-	0	0	Yes	4.03
7-deoxynarciclasine	No	No	No	No	No	-	+	+	-	-	-	0	0	Yes	4.01
5,6-dihydro-5-methyl-2-hydroxyphenanthridine	Yes	No	No	Yes	Yes	-	+	+	-	+	-	0	0	Yes	2.73
3,11-dimethoxy-lycoramine	No	No	No	Yes	No	-	+	+	-	-	-	0	0	Yes	4.36
(2R)-2-methoxy-1,2,3,4-tetrahydro [1,3] dioxolo[4,5-j] phenanthridine	Yes	Yes	No	Yes	Yes	-	+	+	-	+	-	0	0	Yes	3.06
Zephyranthine	No	No	No	Yes	No	-	+	+	-	-	-	0	0	Yes	4.02
Lycoramine	No	No	No	Yes	No	-	+	+	-	-	-	0	0	Yes	4.36
Lycoricidine	No	No	No	No	No	-	+	+	-	-	-	0	0	Yes	4.01
Perlolyrine	Yes	No	No	Yes	Yes	-	+	+	-	-	-	0	0	Yes	2.98
Dihydrolycorine	No	No	No	Yes	No	-	+	+	-	-	-	0	0	Yes	3.99
Anhydrolycorine	Yes	No	No	Yes	Yes	-	+	+	-	+	-	0	0	Yes	2.67
Assoanine	Yes	No	No	Yes	Yes	-	+	+	-	+	+	0	0	Yes	2.68
Cherylline	No	No	No	Yes	No	-	+	+	-	+	-	0	0	Yes	2.88
Epilycoramine	No	No	No	No	No	-	+	+	-	-	-	0	0	Yes	4.36
Narciclasine	No	No	No	No	No	-	+	+	-	-	-	0	0	Yes	4.09
Narwedine	No	No	No	No	No	-	+	+	-	-	-	0	0	Yes	4.29

Table 4. Predicted toxicity profiles of *Lycoris* alkaloids.

	Ames mutagenesis	Acute Oral Toxicity [c]	Eye corrosion	Eye irritation	Hepatotoxicity	Human either-a-go-go inhibition	Micro-nuclear
O-demethyllycoramine	-	III	-	-	-	-	-
7-oxodihydrolycorine	-	III	-	-	-	-	+
7-deoxynarciclasine	+	III	-	-	+	-	+
5,6-dihydro-5-methyl-2-hydroxyphenanthridine	-	III	-	-	+	-	+
3,11-dimethoxy-lycoramine	-	III	-	-	-	-	-
(2R)-2-methoxy-1,2,3,4-tetrahydro [1,3] dioxolo [4,5-j] phenanthridine	+	III	-	-	-	+	-
Zephyranthine	-	III	-	-	-	-	+
Lycoramine	-	III	-	-	-	-	-
Lycoricidine	+	III	-	-	+	-	+
Perlolyrine	+	III	-	-	+	-	+
Dihydrolycorine	-	III	-	-	-	-	+
Anhydrolycorine	-	III	-	-	+	-	+
Assoanine	-	II	-	-	+	+	+
Cherylline	-	III	-	-	-	+	+
Epilycoramine	-	III	-	-	-	-	-
Narciclasine	-	III	-	-	+	-	+
Narwedine	-	III	-	-	-	-	-

The micronucleus test is now recognized as one of the most reliable assays for genotoxic substances. Six *Lycoris* alkaloids were negative for the micronucleus test which are O-demethyllycoramine, 3,11-dimethoxy-lycoramine, (2R)-2-methoxy-1,2,3,4-tetrahydro [1,3] dioxolo[4,5-j] phenanthridine, epilycoramine and narwedine while majority of the compounds were positive for micronucleus test making them potential genotoxic compounds (Table 4).

Based on molecular docking and ADMET prediction results, 4 alkaloids with high docking scores whose complexes showed favorable interactions, drug-likeness, absorption and distribution, metabolism, medicinal chemistry and toxicity were regarded as potential inhibitors of the SARS-CoV-2 Mpro. These compounds are O-demethyllycoramine, 3,11-dimethoxy-lycoramine, epilycoramine and narwedine. 2D structures of the compounds including UAW246, SARS-CoV-2 Mpro 3D structure nd 3D structures of the docked ligands are displayed in Figures 1-5.

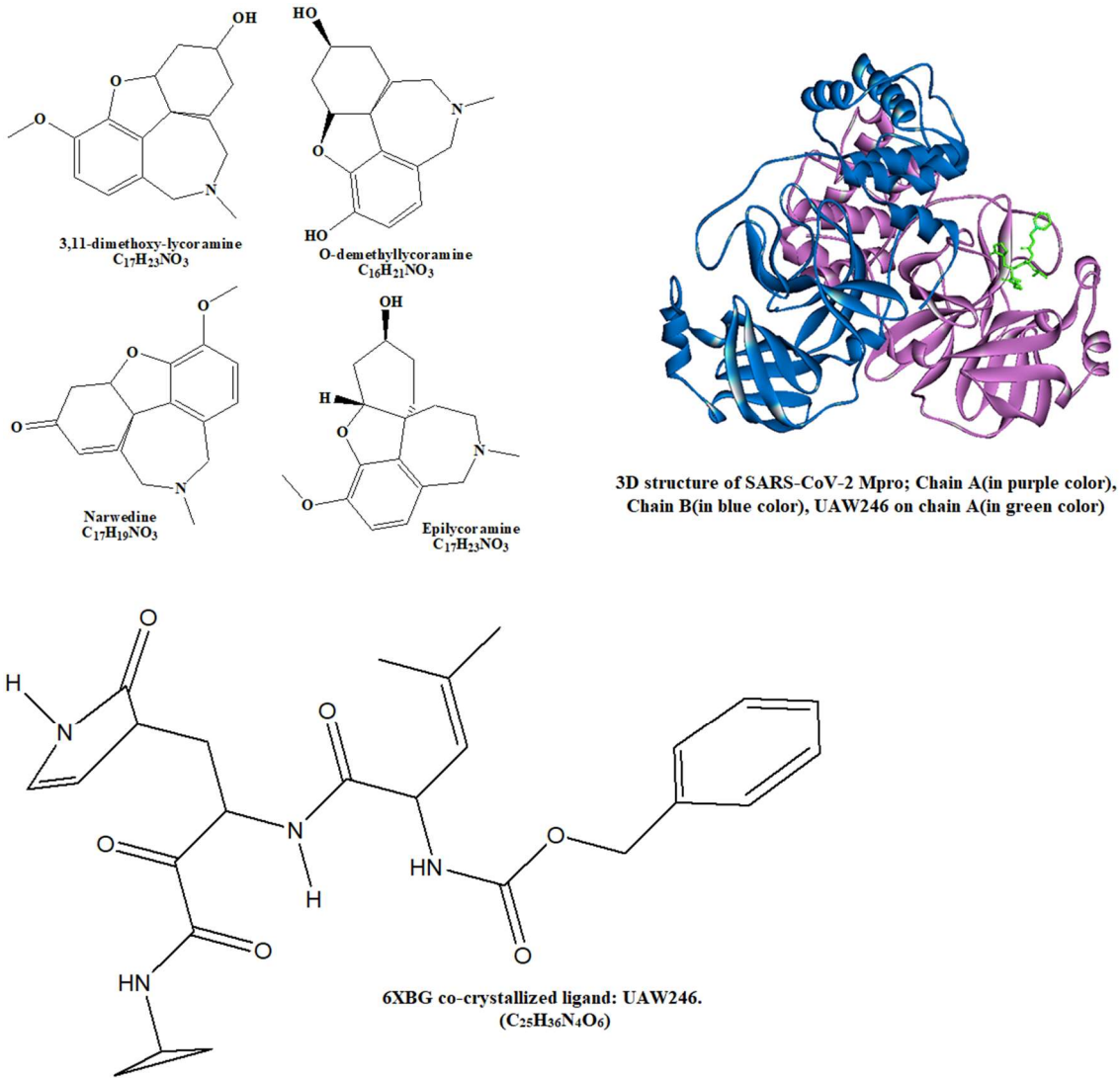

Figure 1. 2D structures of *Lycoris* alkaloids selected for MD simulations, SARS-CoV-2 Mpro 3D structure (showing Chain A and B) and 2D structure of Mpro co-crystallized ligand: UAW 246.

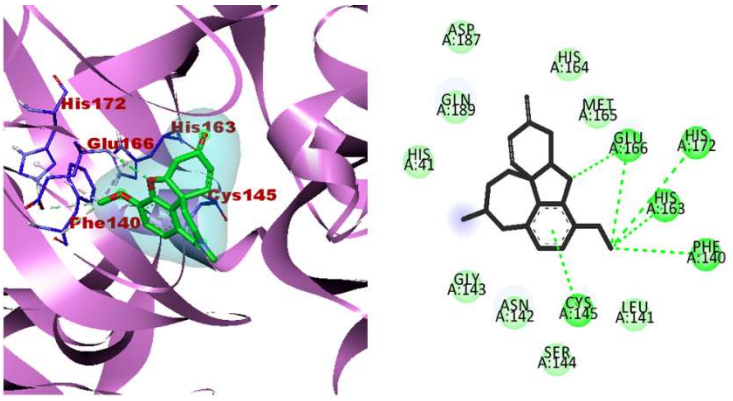

Figure 2. 3, 11-dimethoxy-lycoramine-Mpro interactions include: Van der Waals forces observed in ASP187, GLN189, HIS41, HIS164, MET165, GLY143, ASN142, SER144 and LEU141, conventional hydrogen bond seen in GLU166, pi-donor hydrogen bonds seen in CYS145, pi-Alkyl interactions observed in HIS172 and HIS163 and carbon-hydrogen bonds observed in GLU166 and PHE 140; Binding energy= -7.1 kcalmol^{-1}.

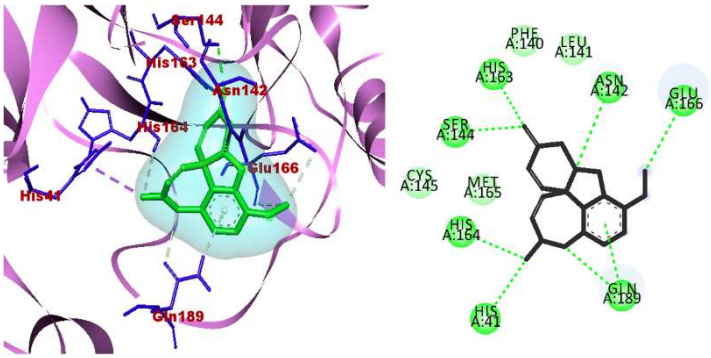

Figure 3. Epilycoramine-Mpro interactions include: Van der Waals forces in PHE 140, LEU141, CYS145 and MET165, conventional hydrogen bonds in HIS 163 and SER 144, pi-donor hydrogen bond in GLN189, pi-sigma in HIS41 and carbon-hydrogen bonds in GLN 189, HIS 164, ASN 142 and GLU166; Binding energy= -6.9 kcalmol^{-1}.

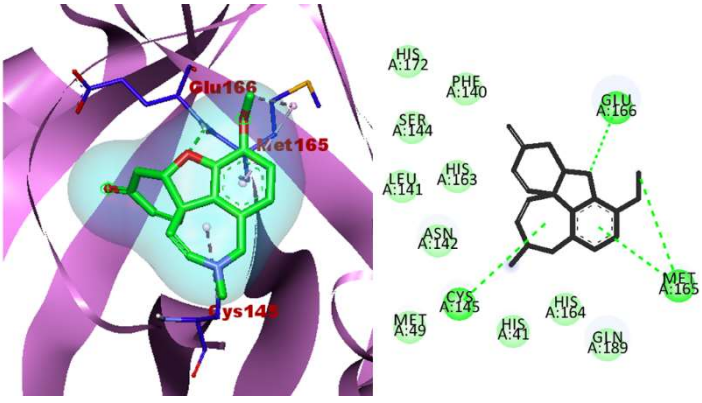

Figure 4. Narwedine-Mpro interactions include: Van der Waals forces observed in HIS172, PHE140, SER144, LEU141, HIS163, ASN142, MET49, HIS41, HIS164 and GLN189, conventional hydrogen bond in GLU166 and pi-Alkyl in both MET145 and CYS145; Binding energy= -6.7 kcalmol^{-1}.

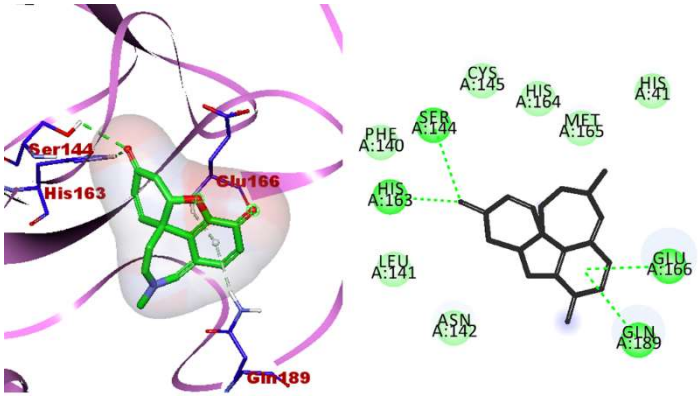

Figure 5. O-demethyllycoramine-Mpro interactions include Van der Waals forces in PHE140, CYS145, HIS164, MET165, HIS41, ASN142 and LEU141, conventional hydrogen bonds in SER144 and HIS163 and pi-Donor hydrogen bonds in GLU166 and GLN189; Binding energy= -7.2 kcalmol^{-1}.

3.3. MD simulations of docked *Lycoris* alkaloids

MD simulations for the four promising *Lycoris* alkaloids were done in WebGro for 100ns. Root mean square deviation of the given structure (RMSD), root mean square fluctuation (RMSF), radius of gyration or structural compactness (Rg), solvent-accessible surface area (SASA) and number of H-bonds in each frame over time of the simulated complexes is shown Figures 6-10. Root mean square deviation (RMSD) computes the average distance between the backbone atoms of starting structure with simulated structures when superimposed [85]. RMSD was plotted to compare the protein backbone stability (Figure 6). The backbones of all the five complexes under investigation showed significant RMSD fluctuations within the first 20 ns of the simulations. In the first 20ns, there were significant fluctuations in RMSD noticed in epilycoramine-Mpro, narwedine-Mpro and 3,11-dimethoxy-lycoramine-Mpro, followed by slight fluctuations in RMSD till the end of simulation time implying the systems for the three compounds reached equilibrium within 20ns. However, O-demethyllycoramine-Mpro and UAW246-Mpro significant fluctuations in RMSD persisted till the end of simulation time. Average RMSD values in Å (1Å = nm*10) for the five complexes were: 3,11-dimethoxy-lycoramine-Mpro (3.1Å), narwedine-Mpro (3.3Å), O-demethyllycoramine-Mpro (3.3Å), epilycoramine-Mpro (3.5Å) and UAW246-Mpro (3.2Å). High average RMSD values implies high fluctuations seen in complexes making them less stable while low RMSD values mean fewer fluctuations and these low values are seen in a more stable complex. Low RMSD values for structure are preferred, a generally acceptable range of the RMSD when a model is overlapped to a template is 2Å [86,87]. But this RMSD cannot be considered as the only criteria for evaluation of MD simulation results. Some deviations at times can be considered [88,89]. Since there is an asymmetry on the functioning of SARS CoV-2 Mpro, ligand binding at one cavity induces conformational changes on the ligand-free pocket and to some extent on the whole receptor [9]. Hence fluctuations in RMSD could also be associated with reorganization of the dimer interface upon considering only one chain was employed for MD simulations.

Fluctuations or standard deviation of atomic positions of each amino acids (residues) in the trajectory were computed and displayed in Figure 7. RMSF values provide insight into structural fluctuations as well as the flexibility of different regions of a protein, if RMSF values are low, it means that the residues are stable, if the RMSF values are high it means the residues are unstable and their atomic positions change more during the simulation time [90]. Average RMSF values (in Å) for the five complexes over the 100 ns were: 3,11-

dimethoxy-lycoramine-Mpro (1.7 Å), narwedine-Mpro (1.6 Å), O-demethyllycoramine-Mpro (1.6 Å), epilycoramine-Mpro (1.6 Å) and UAW246-Mpro (1.8 Å). Most of the proteins' residues in the five complexes showed low RMSF values of ≤1.8 Å and the general shape of the fluctuation's curve for the five complexes was more or less the same (Figure 7) and there were no significant changes in all ligands in the Mpro binding pocket.

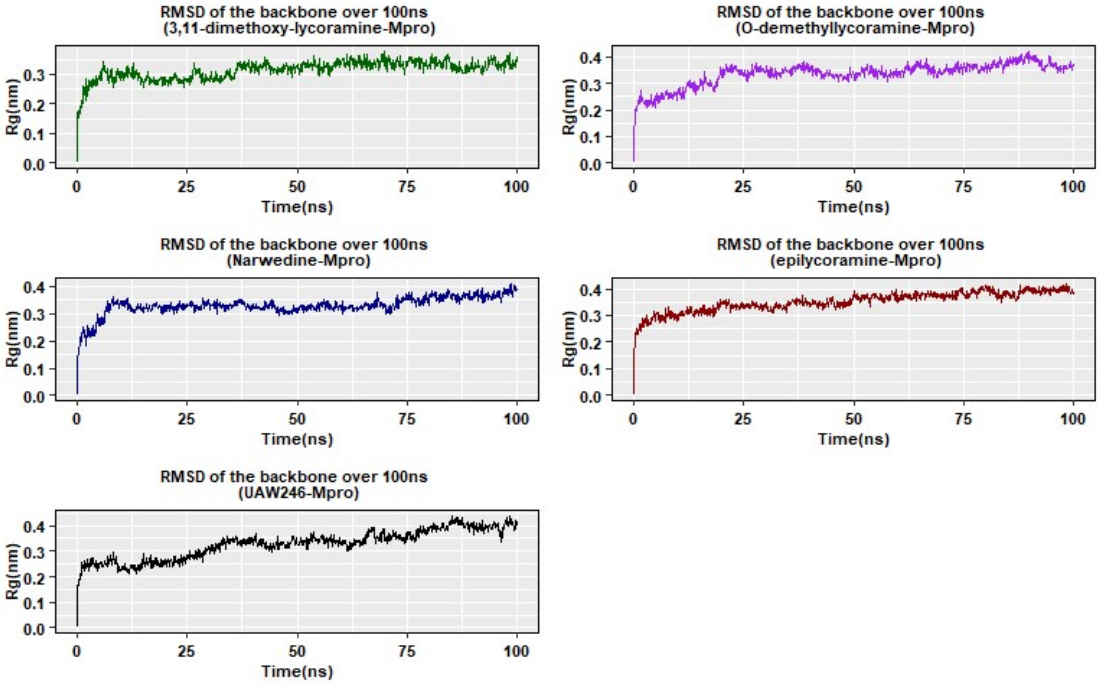

Figure 6. Root mean square deviation (RMSD) of the backbone over 100 ns.

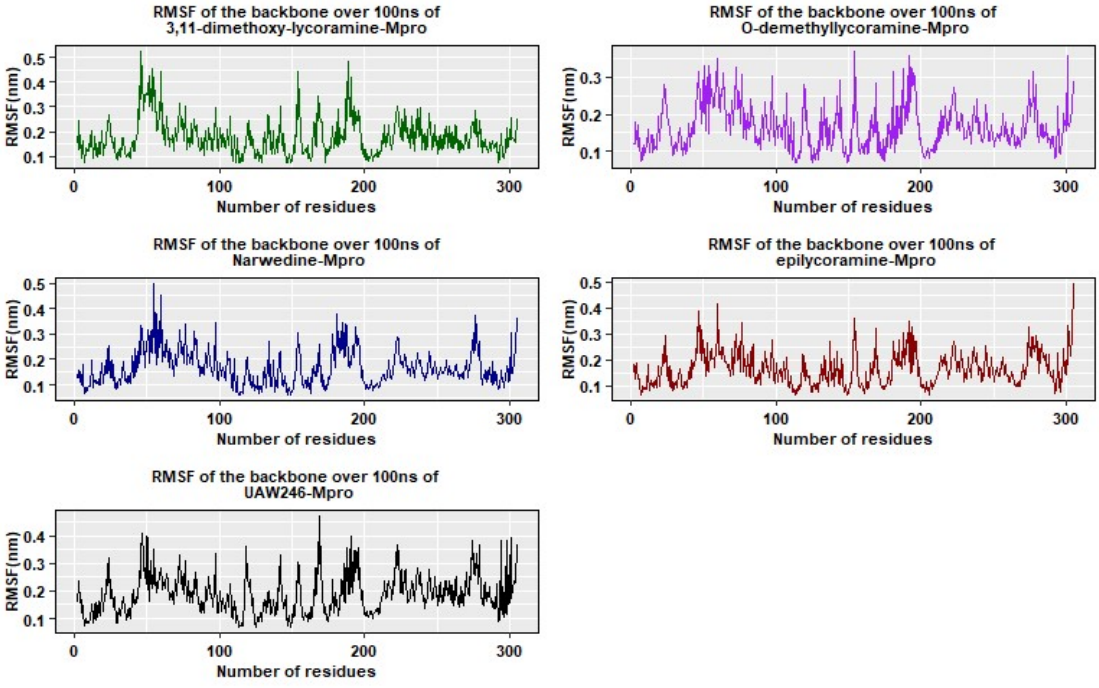

Figure 7. RMSF of the backbone atoms over 100 ns.

Binding stabilities of the protein-ligand complexes were evaluated by calculating the hydrogen bond profiles in GROMACS and the number of hydrogen bonds over time (Figure 8). The analysis revealed that more hydrogen bonds were observed in O-demethylycoramine-Mpro (maximum four hydrogens bonds), epilycoramine-Mpro complex (maximum of three hydrogen bonds) and UAW246-Mpro (maximum three hydrogens bonds), least hydrogen bonds were observed in 3,11-dimethoxy-lycoramine-Mpro, and in narwedine-Mpro complex. It has been argued that a higher number of hydrogens bonds make ligand-receptor complexes more stable [53]. Hence with regard to hydrogen bonding, binding stabilities were higher in O-demethylycoramine-Mpro and epilycoramine-Mpro complexes. However, the overall docking score is not just due to hydrogens bond interactions but due to a cumulative effect of various interactions of the ligand-receptor complex.

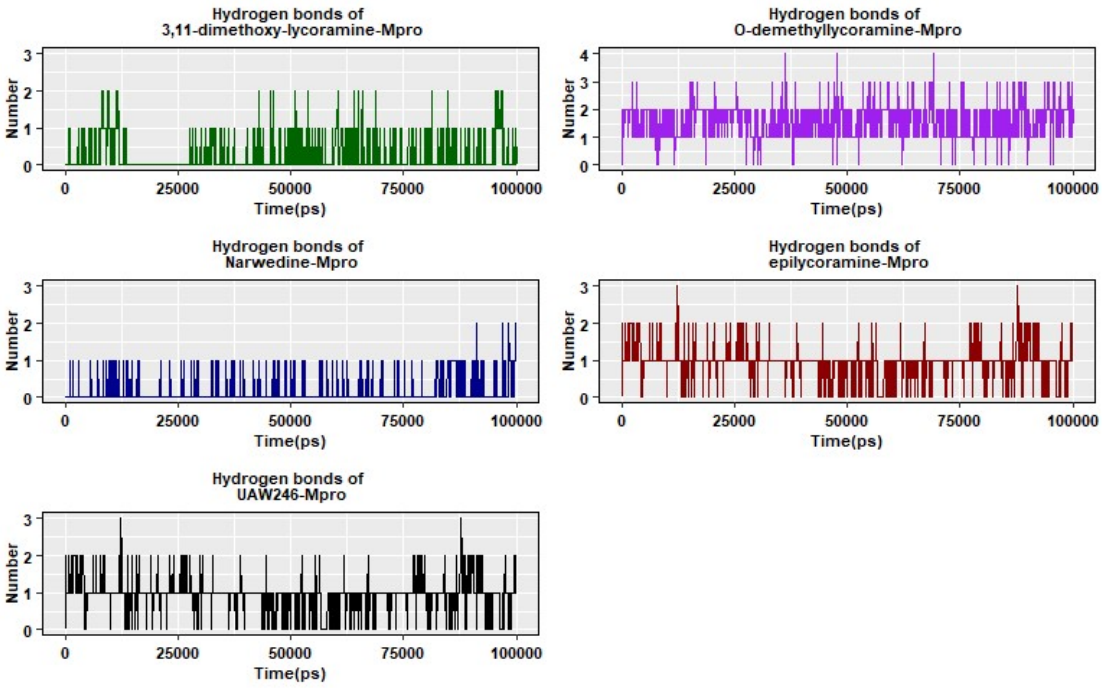

Figure 8. Number of hydrogen bonds over 100 ns.

Radius of gyration (Rg) computes the radius of gyration of a molecule; the radii of gyration about the x-, y- and z-axes, as a function of time [91]. It is a measurement of the distance between the center of mass of the protein atoms with its terminal in a given time frame. Generally, a compact protein or globular protein shows low or less variation in the gyration value while the expanded form of the structure shows a higher Rg value [90]. In the five complexes, the Rg values ranged from 2.58 nm to 2.44 nm. Over the 100 ns simulation time, Rg values in all were seen to decrease from the initial 2.58 nm value. A sharp decrease in Rg is also seen in all the complexes within the first 10ns from 2.58 nm to 2.50 nm. Average Rg values for the five complexes over the 100 ns were: 3,11-dimethoxy-lycoramine-Mpro (2.47 nm), narwedine-Mpro (2.43 nm), O-demethyllycoramine-Mpro (2.44 nm), epilycoramine-Mpro (2.45 nm) and UAW246-Mpro (2.46 nm) (Figure 9). From the average Rg values and the Rg fluctuation curve we can conclude that the structural compactness of the complexes under study was more or less the same over the 100,000 picoseconds (100ns). Reduced Rg values indicates that the complexes became more stable/more compact with increase in simulation time and the reduced Rg values could also be attributed to reorganization of amino acids in the Mpro dimer over the simulation time.

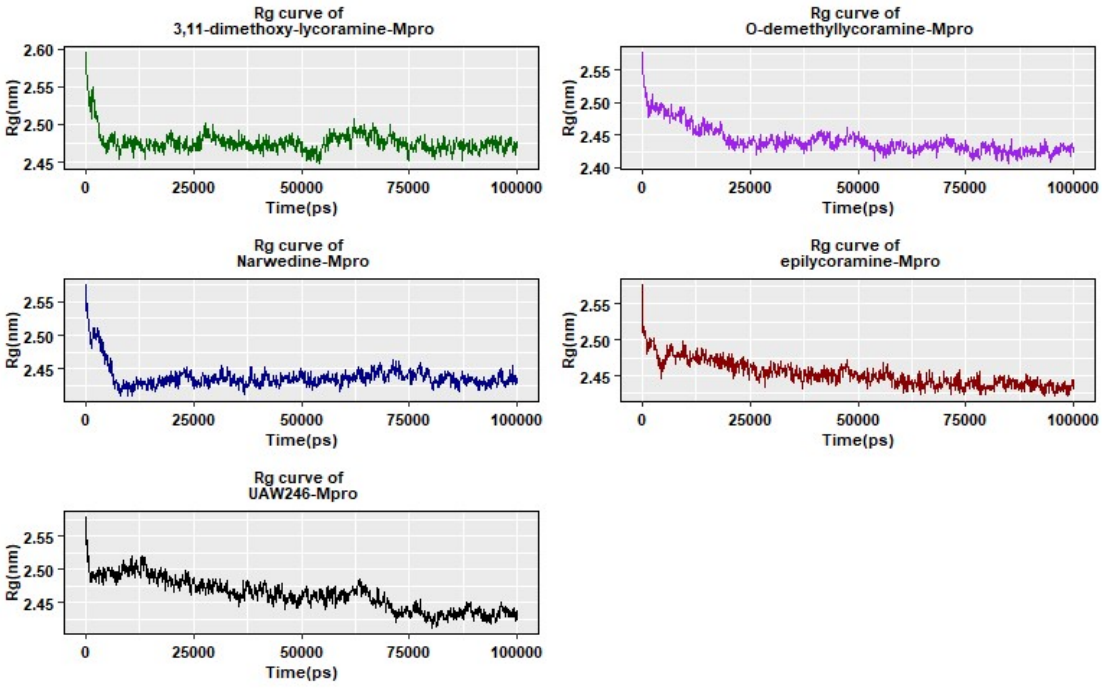

Figure 9. Radius of gyration over 100 ns.

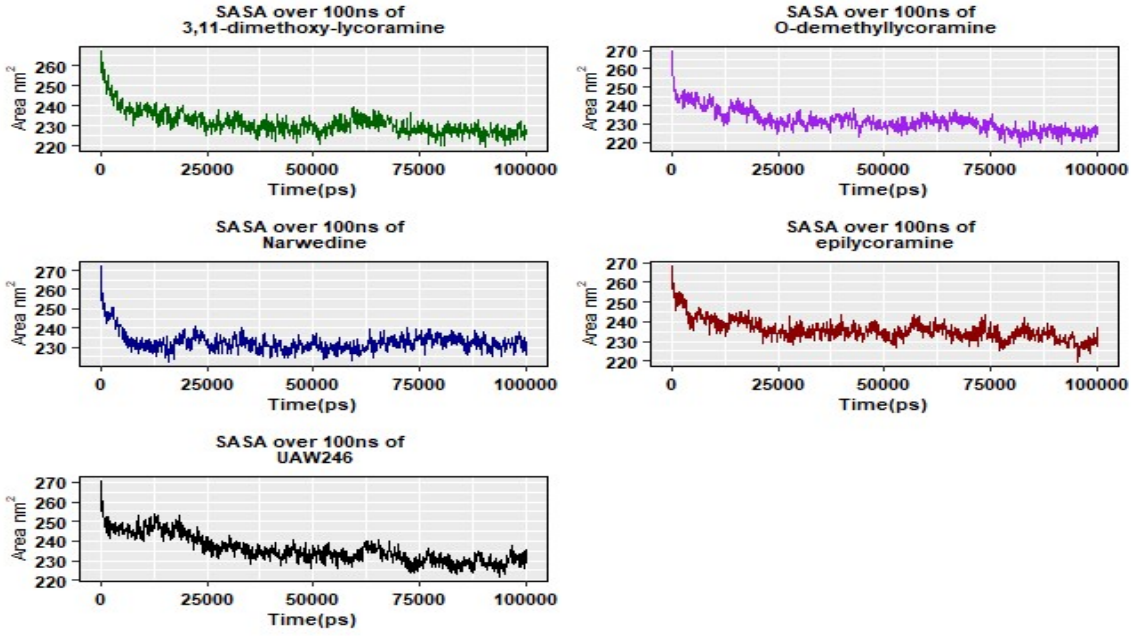

Figure 10. Solvent Accessible Surface Area (SASA) over 100 ns.

Solvent-accessible surface area (SASA) is an approximate surface area of a biomolecule that is accessible to a solvent (in most cases water) with respect to simulation time [92]. Average SASA values (nm^2) over the 100 ns for 3,11-dimethoxy-lycoramine, narwedine, O-demethyllycoramine, epilycoramine and UAW246 were 231.37 nm^2, 232.39 nm^2, 231.35 nm^2, 235.63 nm^2 and 235.62 nm^2 respectively (Figure 10). Lower SASA implies that the ligand is consistent and doesn't shift much in its binding pocket [93]. Hence 3,11-dimethoxy-lycoramine and O-demethyllycoramine with lower SASA implied that the two ligands were more stable and consistent in the binding pocket of SARS-CoV-2 Mpro compared to the other ligands under study

which stuck out to solvent and have higher SASA. Generally, SASA for the five ligands was seen to decrease over the 100ns meaning the ligands did not shift much in their binding pockets and less of their surfaces were exposed to solvent with an increase in simulation time. Similarly, a decrease in SASA over the simulation time can be a consequence of the reorganization of Mpro ligand binding regions.

Drug development process is constantly experiencing issues in rising costs and achieving FDA approval [94]. Novel approaches are essential to identify drug targets correctly and perform efficacy predictions with ease. *In silico* computational approaches provide means to qualitatively and quantitatively investigate various treatments on specific diseases on a wider scale by subjecting such treatment to different conditions prior to *in vitro*/*vivo* evaluation, and this allows optimization during drug development. *In silico* methods such as pharmacophore modelling, Quantitative Structure Activity Relationship (QSAR), Scaffold hopping and molecular docking are some of the methods of rapidly screening extensive libraries of ligands and targets and offer various solutions to current problems in drug development [95]. Generally, *in silico* methods offer more practical and cost-effective experiments, are less expensive, less time consuming, allow constant drug optimization, have higher reproducibility and have low compound synthesis requirements. Furthermore, computer aided drug design methods limit the use of animal models in research which supports the idea of designing novel and safe drug candidates [96,97].

One of the main drawbacks of *in silico* methods is ensuring appropriate scoring functions and algorithms for molecular screening are implemented to ensure accuracy of these methods. Nevertheless, post-processing algorithms with more accurate scoring functions have been developed [98,99]. Another limitation of *in silico* methods is the complexity of molecular dynamics. Performing MD simulations is computationally-demanding, requires ultra-fast computers and is dependent on the size of the simulated systems and the some longest reported analysis periods range from hundred nanoseconds to microseconds. Such a limited time period is often too short to simulate most of the interactions seen in molecular docking experiments and this leads to generation of inadequate and unreliable MD simulation results [100,101].

4. CONCLUSIONS

MD simulation analysis showed that RMSD and RMSF for the five compounds did not fluctuate much over the simulation time except for O-demethyllycoramine-Mpro and UAW246-Mpro. With regard to Rg and SASA, a decrease in Rg and SASA over time was observed in all the five docked compounds pointing to more compact and stable complexes. However, a higher number of hydrogens bonds was observed in O-demethylycoramine-Mpro, epilycoramine-Mpro and UAW246-Mpro complexes compared to 3,11-dimethoxy-lycoramine-Mpro and narwedine-Mpro complexes. MD simulation analysis revealed that although the four *Lycoris* alkaloids besides UAW246 formed stable complexes with SARS-CoV-2 Mpro, higher stability was observed in O-demethylycoramine-Mpro, epilycoramine-Mpro and UAW246-Mpro over 100 ns simulation time. The study indicates that the four *Lycoris* alkaloids are drug-like and lead-like compounds with favorable ADMET properties and are very likely to have an inhibition potential against SARS-CoV-2 and may become potential drug candidates. However, further *in vitro* and *in vivo* studies of the four *Lycoris* alkaloids are required to validate these findings.

Abbreviations:

ADMET, absorption, distribution, metabolism, elimination and toxicity; BBB, blood-brain barrier; COVID-19, coronavirus disease 2019; CYP, cytochrome P450; GI, gastrointestinal absorption; hERG, Human Ether-à-go-

go-Related Gene; MATE1, multidrug and toxin extrusion 1; MD, molecular dynamic simulations; Mpro, main protease; OATP, organic anion transporting polypeptide; OCT; organic cationic transporter; PAINS, pan assay interference compounds; P-gp, p glycoprotein; PPB, plasma protein binding; Rg, radius of gyration; RMSD, root mean square deviation; RMSF, root mean square fluctuation; SARS-CoV-2, severe acute respiratory syndrome coronavirus 2; SASA, solvent accessible surface area.

Authors' Contributions: The following authors contributed to this study: conceptualization, F.M. M, G.W.G and M.M.K; methodology, F.M.M. D.B.K and M.M.K.; data analysis, F.M.M and J.M.M; writing-original draft preparation, F.M.M, D.B.K and G.W.G; writing- review and editing, F.M.M, J.M.N, M.M.K and J.M.M. All authors read and approved the final version of the manuscript.

Conflict of Interest: The authors declare no conflict of interest.

Funding: This research was not funded by any organization

REFERENCES

1. Paules CI, Marston HD, Fauci AS. Coronavirus infections - more than just the common cold. JAMA. 2020;323(8):707-8.
2. WHO. COVID-19 Weekly Epidemiological Update 35. World Heal Organ. 2021:1-3. Available from: https://www.who.int/docs/default-source/coronaviruse/situation-reports/weekly_epidemiological_update_22.pdf
3. Zhou P, Yang X-L, Wang X-G, Hu B, Zhang L, Zhang W, et al. A pneumonia outbreak associated with a new coronavirus of probable bat origin. Nature. 2020;579(7798):270-3.
4. Chan JF-W, Kok K-H, Zhu Z, Chu H, To KK-W, Yuan S, et al. Genomic characterization of the 2019 novel human-pathogenic coronavirus isolated from a patient with atypical pneumonia after visiting Wuhan. Emerg Microbes Infect. 2020;9(1):221-36.
5. Nicola M, Alsafi Z, Sohrabi C, Kerwan A, Al-Jabir A, Iosifidis C, et al. The socio-economic implications of the coronavirus pandemic (COVID-19): A review. Int J Surg. 2020;78:185-93.
6. Wouters OJ, Shadlen KC, Salcher-Konrad M, Pollard AJ, Larson HJ, Teerawattananon Y, et al. Challenges in ensuring global access to COVID-19 vaccines: production, affordability, allocation, and deployment. Lancet. 2021;397(10278):P1023-34.
7. Forni G, Mantovani A. COVID-19 vaccines: where we stand and challenges ahead. Cell Death Differ. 2021;28(2):626-39.
8. Perlman S, Netland J. Coronaviruses post-SARS: update on replication and pathogenesis. Nat Rev Microbiol. 2009;7(6):439-50.
9. Jin Z, Du X, Xu Y, Deng Y, Liu M, Zhao Y, et al. Structure of M pro from SARS-CoV-2 and discovery of its inhibitors. Nature. 2020;582(7811):289-93.
10. Ullrich S, Nitsche C. The SARS-CoV-2 main protease as drug target. Bioorg Med Chem Lett. 2020;127377.
11. Wu A, Peng Y, Huang B, Ding X, Wang X, Niu P, et al. Genome composition and divergence of the novel coronavirus (2019-nCoV) originating in China. Cell Host Microbe. 2020;27(3):325-8.
12. Du Q-S, Wang S-Q, Zhu Y, Wei D-Q, Guo H, Sirois S, et al. Polyprotein cleavage mechanism of SARS CoV Mpro and chemical modification of the octapeptide. Peptides. 2004;25(11):1857-64.
13. Agbowuro AA, Huston WM, Gamble AB, Tyndall JDA. Proteases and protease inhibitors in infectious diseases. Med Res Rev. 2018;38(4):1295-331.

14. Zhang L, Lin D, Sun X, Curth U, Drosten C, Sauerhering L, et al. Crystal structure of SARS-CoV-2 main protease provides a basis for design of improved α-ketoamide inhibitors. Science. 2020;368(6489):409-12.
15. Chen YW, Yiu C-PB, Wong K-Y. Prediction of the SARS-CoV-2 (2019-nCoV) 3C-like protease (3CL pro) structure: virtual screening reveals velpatasvir, ledipasvir, and other drug repurposing candidates. F1000Research. 2020;9.
16. Zhang Y-N, Zhang Q-Y, Li X-D, Xiong J, Xiao S-Q, Wang Z, et al. Gemcitabine, lycorine and oxysophoridine inhibit novel coronavirus (SARS-CoV-2) in cell culture. Emerg Microbes Infect. 2020;9(1):1170-3.
17. Cahlíková L, Breiterová K, Opletal L. Chemistry and biological activity of alkaloids from the genus Lycoris (Amaryllidaceae). Molecules. 2020;25(20):4797.
18. Chen G-L, Tian Y-Q, Wu J-L, Li N, Guo M-Q. Antiproliferative activities of Amaryllidaceae alkaloids from Lycoris radiata targeting DNA topoisomerase I. Sci Rep. 2016;6(1):1-10.
19. Feng T, Wang Y, Su J, Li Y, Cai X, Luo X. Amaryllidaceae alkaloids from Lycoris radiata. Helv Chim Acta. 2011;94(1):178-83.
20. Hao B, Shen S-F, Zhao Q-J. Cytotoxic and antimalarial amaryllidaceae alkaloids from the bulbs of Lycoris radiata. Molecules. 2013;18(3):2458-68.
21. Liu Z-M, Huang X-Y, Cui M-R, Zhang X-D, Chen Z, Yang B-S, et al. Amaryllidaceae alkaloids from the bulbs of Lycoris radiata with cytotoxic and anti-inflammatory activities. Fitoterapia. 2015;101:188-93.
22. Toriizuka Y, Kinoshita E, Kogure N, Kitajima M, Ishiyama A, Otoguro K, et al. New lycorine-type alkaloid from Lycoris traubii and evaluation of antitrypanosomal and antimalarial activities of lycorine derivatives. Bioorg Med Chem. 2008;16(24):10182-9.
23. Jin A, Li X, Zhu Y-Y, Yu H-Y, Pi H-F, Zhang P, et al. Four new compounds from the bulbs of Lycoris aurea with neuroprotective effects against CoCl 2 and H 2 O 2-induced SH-SY5Y cell injuries. Arch Pharm Res. 2014;37(3):315-23.
24. Zhu Y-Y, Li X, Yu H-Y, Xiong Y-F, Zhang P, Pi H-F, et al. Alkaloids from the bulbs of Lycoris longituba and their neuroprotective and acetylcholinesterase inhibitory activities. Arch Pharm Res. 2015;38(5):604-13.
25. Guo Y, Pigni NB, Zheng Y, de Andrade JP, Torras-Claveria L, de Souza Borges W, et al. Analysis of bioactive Amaryllidaceae alkaloid profiles in Lycoris species by GC-MS. Nat Prod Commun. 2014;9(8):1934578X1400900806.
26. Tian Y, Zhang C, Guo M. Comparative analysis of Amaryllidaceae alkaloids from three Lycoris species. Molecules. 2015;20(12):21854-69.
27. Sun Z-F, Mu S-Z, Ge Y-H, Hao X-J. Alkaloid type analysis of Lycoris radiata and Lycoris aurea using GC-MS method. J Mt Agric Biol. 2012;2:22.
28. Li A, Du Z, Liao M, Feng Y, Ruan H, Jiang H. Discovery and characterisation of lycorine-type alkaloids in Lycoris spp.(Amaryllidaceae) using UHPLC-QTOF-MS. Phytochem Anal. 2019;30(3):268-77.
29. Cao Z, Yang P, Zhou Q. Multiple biological functions and pharmacological effects of lycorine. Sci China Chem. 2013;56(10):1382-91.
30. Kim S, Thiessen PA, Bolton EE, Chen J, Fu G, Gindulyte A, et al. PubChem substance and compound databases. Nucleic Acids Res. 2016;44(D1):D1202-13.
31. Gaulton A, Hersey A, Nowotka M, Bento AP, Chambers J, Mendez D, et al. The ChEMBL database in 2017. Nucleic Acids Res. 2017;45(D1):D945-54.
32. Mendelsohn LD. ChemDraw 8 ultra, windows and macintosh versions. J Chem Inf Comput Sci. 2004;44(6):2225-6.
33. Biovia DS. Discovery studio visualizer. San Diego, CA, USA. 2017;936.
34. Baell JB, Holloway GA. New substructure filters for removal of pan assay interference compounds (PAINS) from screening libraries and for their exclusion in bioassays. J Med Chem. 2010;53(7):2719-40.

35. Baell JB, Ferrins L, Falk H, Nikolakopoulos G. PAINS: Relevance to tool compound discovery and fragment-based screening. Aust J Chem. 2013;66(12):1483-94.
36. Brenk R, Schipani A, James D, Krasowski A, Gilbert IH, Frearson J, et al. Lessons learnt from assembling screening libraries for drug discovery for neglected diseases. ChemMedChem. 2008;3(3):435.
37. Daina A, Michielin O, Zoete V. SwissADME: a free web tool to evaluate pharmacokinetics, drug-likeness and medicinal chemistry friendliness of small molecules. Sci Rep. 2017;7(1):1-13.
38. Pettersen EF, Goddard TD, Huang CC, Couch GS, Greenblatt DM, Meng EC, et al. UCSF Chimera—a visualization system for exploratory research and analysis. J Comput Chem. 2004;25(13):1605-12.
39. Dallakyan S, Olson AJ. Small-molecule library screening by docking with PyRx. In: Chemical biology. Springer; 2015. p. 243-50.
40. Cheng F, Li W, Zhou Y, Shen J, Wu Z, Liu G, et al. admetSAR: a comprehensive source and free tool for assessment of chemical ADMET properties. ACS Publications; 2012.
41. Kumari A, Mittal L, Srivastava M, Asthana S. Binding mode characterization of 13b in the monomeric and dimeric states of SARS-CoV-2 main protease using molecular dynamics simulations. J Biomol Struct Dyn. 2021;1-19.
42. Schüttelkopf AW, Van Aalten DMF. PRODRG: a tool for high-throughput crystallography of protein-ligand complexes. Acta Crystallogr Sect D Biol Crystallogr. 2004;60(8):1355-63.
43. Ren P, Shang W, Yin W, Ge H, Wang L, Zhang X, et al. A multi-targeting drug design strategy for identifying potent anti-SARS-CoV-2 inhibitors. Acta Pharmacol Sin. 2021;1-11.
44. Wang H, Wang Y, Zhao F, Huang Q, Jinjin XU, Lijuan MA, et al. Benzylphenethylamine alkaloids from the bulbs and flowers of Lycoris radiata. Chinese Herb Med. 2011;3(1):60-3.
45. Yin S, Qiu Y, Jin C, Wang R, Wu S, Liu H, et al. 7-Deoxynarciclasine shows promising antitumor efficacy by targeting Akt against hepatocellular carcinoma. Int J cancer. 2019;145(12):3334-46.
46. Ang S, Liu X-M, Huang X-J, Zhang D-M, Zhang W, Wang L, et al. Four new Amaryllidaceae alkaloids from Lycoris radiata and their cytotoxicity. Planta Med. 2015;81(18):1712-8.
47. HU Y, MU S, YAN C, SUN Z, ZHANG J, HAO X. Isolation and identification of alkaloids of bulbs of Lycoris radiata Herb. produced in Guizhou province. J Shenyang Pharm Univ. 2013;
48. Mu H, Wang R, Li X, Jiang Y, Peng F, Xia B. Alkaloid accumulation in different parts and ages of Lycoris chinensis. Zeitschrift für Naturforsch C. 2010;65(7-8):458-62.
49. Yang D-Q, Chen Z-R, Chen D-Z, Hao X-J, Li S-L. Anti-TMV effects of Amaryllidaceae alkaloids isolated from the bulbs of Lycoris radiata and Lycoricidine derivatives. Nat Products Bioprospect. 2018;8(3):189-97.
50. Huan W, Yue-hu W, Li-juan C, Chun-lin L. Research Progress of Alkaloids from Lycoris. Nat Prod Res Dev. 2012;24(5):1102-6.
51. Shen C-Y, Xu X-L, Yang L-J, Jiang J-G. Identification of narciclasine from Lycoris radiata (L'Her.) Herb. and its inhibitory effect on LPS-induced inflammatory responses in macrophages. Food Chem Toxicol. 2019;125:605-13.
52. Jianxin SZMSZ, Xiaojiang YCHLH. Chemical constituents of Lycoris aurea from Guizhou province. J North Pharm. 2013;
53. Chen D, Oezguen N, Urvil P, Ferguson C, Dann SM, Savidge TC. Regulation of protein-ligand binding affinity by hydrogen bond pairing. Sci Adv. 2016;2(3):e1501240.
54. Ramírez D, Caballero J. Is it reliable to take the molecular docking top scoring position as the best solution without considering available structural data? Molecules. 2018;23(5):1038.
55. Yoshino R, Yasuo N, Sekijima M. Identification of key interactions between SARS-CoV-2 main protease and inhibitor drug candidates. Sci Rep. 2020;10(1):1-8.

56. Lipinski CA, Lombardo F, Dominy BW, Feeney PJ. Experimental and computational approaches to estimate solubility and permeability in drug discovery and development settings. Adv Drug Deliv Rev. 1997;23(1-3):3-25.
57. Ghose AK, Viswanadhan VN, Wendoloski JJ. A knowledge-based approach in designing combinatorial or medicinal chemistry libraries for drug discovery. 1. A qualitative and quantitative characterization of known drug databases. J Comb Chem. 1999;1(1):55-68.
58. Veber DF, Johnson SR, Cheng H-Y, Smith BR, Ward KW, Kopple KD. Molecular properties that influence the oral bioavailability of drug candidates. J Med Chem. 2002;45(12):2615-23.
59. Egan WJ, Merz KM, Baldwin JJ. Prediction of drug absorption using multivariate statistics. J Med Chem. 2000;43(21):3867-77.
60. Muegge I, Heald SL, Brittelli D. Simple selection criteria for drug-like chemical matter. J Med Chem. 2001;44(12):1841-6.
61. Jain KK. Nanobiotechnology-based strategies for crossing the blood-brain barrier. Nanomedicine. 2012;7(8):1225-33.
62. Finch A, Pillans P. P-glycoprotein and its role in drug-drug interactions. Aust Prescr. 2014;37(4):137-9.
63. Huwyler J, Wright MB, Gutmann H, Drewe J. Induction of cytochrome P450 3A4 and P-glycoprotein by the isoxazolyl-penicillin antibiotic flucloxacillin. Curr Drug Metab. 2006;7(2):119-26.
64. Davis TP, Sanchez-Covarubias L, Tome ME. P-glycoprotein trafficking as a therapeutic target to optimize CNS drug delivery. Adv Pharmacol. 2014;71:25-44.
65. Fink-Gremmels J. Implications of hepatic cytochrome P450-related biotransformation processes in veterinary sciences. Eur J Pharmacol. 2008;585(2-3):502-9.
66. Inglese C, Grazia Perrone M, Berardi F, Perrone R, Antonio Colabufo N. Modulation and absorption of xenobiotics: the synergistic role of CYP450 and P-gp activities in cancer and neurodegenerative disorders. Curr Drug Metab. 2011;12(8):702-12.
67. Westervelt P, Cho K, Bright DR, Kisor DF. Drug-gene interactions: inherent variability in drug maintenance dose requirements. Pharm Ther. 2014;39(9):630.
68. Zhou S, Chan SY, Goh BC, Chan E, Duan W, Huang M, et al. Mechanism-based inhibition of cytochrome P450 3A4 by therapeutic drugs. Clin Pharmacokinet. 2005;44(3):279-304.
69. Lynch T, Price AL. The effect of cytochrome P450 metabolism on drug response, interactions, and adverse effects. Am Fam Physician. 2007;76(3):391-6.
70. Müller F, König J, Hoier E, Mandery K, Fromm MF. Role of organic cation transporter OCT2 and multidrug and toxin extrusion proteins MATE1 and MATE2-K for transport and drug interactions of the antiviral lamivudine. Biochem Pharmacol. 2013;86(6):808-15.
71. Yonezawa A, Inui K. Importance of the multidrug and toxin extrusion MATE/SLC47A family to pharmacokinetics, pharmacodynamics/toxicodynamics and pharmacogenomics. Br J Pharmacol. 2011;164(7):1817-25.
72. Szabo M, Veres Z, Baranyai Z, Jakab F, Jemnitz K. Comparison of human hepatoma HepaRG cells with human and rat hepatocytes in uptake transport assays in order to predict a risk of drug induced hepatotoxicity. PLoS One. 2013;8(3):e59432.
73. Clarke JD, Cherrington NJ. Genetics or environment in drug transport: the case of organic anion transporting polypeptides and adverse drug reactions. Expert Opin Drug Metab Toxicol. 2012;8(3):349-60.
74. Shitara Y. Clinical importance of OATP1B1 and OATP1B3 in drug-drug interactions. Drug Metab Pharmacokinet. 2010;1101310150.

75. Gozalpour E, Greupink R, Wortelboer HM, Bilos A, Schreurs M, Russel FGM, et al. Interaction of digitalis-like compounds with liver uptake transporters NTCP, OATP1B1, and OATP1B3. Mol Pharm. 2014;11(6):1844-55.
76. Koepsell H, Lips K, Volk C. Polyspecific organic cation transporters: structure, function, physiological roles, and biopharmaceutical implications. Pharm Res. 2007;24(7):1227-51.
77. Ito K, Suzuki H, Horie T, Sugiyama Y. Apical/basolateral surface expression of drug transporters and its role in vectorial drug transport. Pharm Res. 2005;22(10):1559-77.
78. Shikata E, Yamamoto R, Takane H, Shigemasa C, Ikeda T, Otsubo K, et al. Human organic cation transporter (OCT1 and OCT2) gene polymorphisms and therapeutic effects of metformin. J Hum Genet. 2007;52(2):117-22.
79. Gatehouse D. Bacterial mutagenicity assays: test methods. In: Genetic Toxicology. Springer; 2012. p. 21-34.
80. Bhatia S, Schultz T, Roberts D, Shen J, Kromidas L, Api AM. Comparison of cramer classification between toxtree, the OECD QSAR toolbox and expert judgment. Regul Toxicol Pharmacol. 2015;71(1):52-62.
81. Cramer GM, Ford RA, Hall RL. Estimation of toxic hazard - a decision tree approach. Food Cosmet Toxicol. 1976;16(3):255-76.
82. Perissinotti LL, Guo J, De Biase PM, Clancy CE, Duff HJ, Noskov SY. Kinetic model for NS1643 drug activation of WT and L529I variants of Kv11. 1 (hERG1) potassium channel. Biophys J. 2015;108(6):1414-24.
83. Lamothe SM, Guo J, Li W, Yang T, Zhang S. The human ether-a-go-go-related gene (hERG) potassium channel represents an unusual target for protease-mediated damage. J Biol Chem. 2016;291(39):20387-401.
84. Emam AN, Girgis E, Khalil WKB, Mohamed MB. Toxicity of plasmonic nanomaterials and their hybrid nanocomposites. In: Advances in molecular toxicology. Elsevier; 2014. p. 173-202.
85. Kuzmanic A, Zagrovic B. Determination of ensemble-average pairwise root mean-square deviation from experimental B-factors. Biophys J. 2010;98(5):861-71.
86. Carugo O, Pongor S. A normalized root-mean-spuare distance for comparing protein three-dimensional structures. Protein Sci. 2001;10(7):1470-3.
87. Krippahl L, Moura JJ, Palma PN. Modeling protein complexes with BiGGER. Proteins Struct Funct Bioinforma. 2003;52(1):19-23.
88. Kirchmair J, Markt P, Distinto S, Wolber G, Langer T. Evaluation of the performance of 3D virtual screening protocols: RMSD comparisons, enrichment assessments, and decoy selection—what can we learn from earlier mistakes? J Comput Aided Mol Des. 2008;22(3):213-28.
89. Smith GR, Sternberg MJE, Bates PA. The relationship between the flexibility of proteins and their conformational states on forming protein-protein complexes with an application to protein-protein docking. J Mol Biol. 2005;347(5):1077-101.
90. Aouidate A, Ghaleb A, Chtita S, Aarjane M, Ousaa A, Maghat H, et al. Identification of a novel dual-target scaffold for 3CLpro and RdRp proteins of SARS-CoV-2 using 3D-similarity search, molecular docking, molecular dynamics and ADMET evaluation. J Biomol Struct Dyn. 2020;1-14.
91. Lobanov MY, Bogatyreva NS, Galzitskaya O V. Radius of gyration as an indicator of protein structure compactness. Mol Biol. 2008;42(4):623-8.
92. Durham E, Dorr B, Woetzel N, Staritzbichler R, Meiler J. Solvent accessible surface area approximations for rapid and accurate protein structure prediction. J Mol Model. 2009;15(9):1093-108.
93. Wang J, Wang W, Huo S, Lee M, Kollman PA. Solvation model based on weighted solvent accessible surface area. J Phys Chem B. 2001;105(21):5055-67.
94. Van Norman GA. Drugs, devices, and the FDA: part 1: an overview of approval processes for drugs. JACC Basic to Transl Sci. 2016;1(3):170-9.

95. Surabhi S, Singh BK. Computer aided drug design: an overview. J Drug Deliv Ther. 2018;8(5):504-9.
96. Zoete V, Grosdidier A, Michielin O. Docking, virtual high throughput screening and in silico fragment-based drug design. J Cell Mol Med. 2009;13(2):238-48.
97. Wadood A, Ahmed N, Shah L, Ahmad A, Hassan H, Shams S. In-silico drug design: An approach which revolutionarised the drug discovery process. OA Drug Des Deliv. 2013;1(1):3.
98. Lavecchia A, Cerchia C. In silico methods to address polypharmacology: current status, applications and future perspectives. Drug Discov Today. 2016;21(2):288-98.
99. Lavecchia A, Di Giovanni C. Virtual screening strategies in drug discovery: a critical review. Curr Med Chem. 2013;20(23):2839-60.
100. Casciuc I, Horvath D, Gryniukova A, Tolmachova KA, Vasylchenko O V, Borysko P, et al. Pros and cons of virtual screening based on public “Big Data”: In silico mining for new bromodomain inhibitors. Eur J Med Chem. 2019;165:258-72.
101. Dubey KD, Ojha RP. Molecular dynamics simulations: Applicability and scopes in computational biochemistry. Nanosci Comput Chem Res Prog. 2013;371.